Supplementary Information

Structure and mechanism of a bacterial sodium-dependent dicarboxylate transporter

Romina Mancusso, G. Glenn Gregorio, Qun Liu and Da-Neng Wang

Supplementary Discussion

Transport mechanism

Combination of the crystal structure and transport and binding assays of the vcINDY presented here, along with previous biochemical characterization of its bacterial, fly and, in particular, mammalian homologs [1-4], suggest a transport mechanism for the Na^+-dependent dicarboxylate transporter from *Vibrio cholerae* (Supplementary Fig. 17). In the "substrate-waiting," outward-facing C_o conformation, the transporter adopts a structure in which its N-terminal half is in the "U-shape" while the C-terminal half is in the "V-shape", N(U)-C(V), with its Na^+- and substrate-binding sites facing the extracellular space. Following the induction of the proper substrate pocket by the binding of Na^+ ions, probably two, a substrate molecule binds to the transporter, yielding the C_o-S-Na^+ state. Using the binding energy and aided by Brownian motion, the transporter converts to the C_i-S-Na^+ state. In this state, the palm of the N-terminal half moves toward the cytosol, whereas its thumb stays at its original position in the membrane, yielding an inverted V-shape. At the same time, the C-terminal half of the transporter changes from the V-shape to a U-shape. In this N(V)-C(U) structure, the substrate is exposed to the cytosolic space. Substrate release to the cytosol is then triggered by the escape of the Na2 ion, and is followed by the release of the Na1 ion. Finally, the transporter returns from this C_i state back to the C_o state.

Several pieces of published experimental data on various INDY proteins support the above transport mechanism. Transport kinetics studies on both the rabbit and the human NaDC1 support a binding order of three Na^+ ions from the extracellular space, followed by dicarboxylate [5,6]. Similar observations have been made for the sequence of binding of the two Na^+ ions and one substrate for bacterial INDY homologs [7-9]. Accessibility studies of cysteine substitution in

mammalian NaDC1 using a membrane-impermeable sulfonate reagent have shown that the tip of HP_{out}, including its SNT motif, is accessible from the extracellular space [10-12]. Such accessibility of the hairpin tip is increased in the presence of Na^+ ions, but access to the cysteine labeling is protected by the addition of substrate [11,12]. The equivalent of another segment near the substrate binding site, Ser200 – Pro202 in vcINDY, has also been found to be accessible from the extracellular side in the human sulfate transporter NaS1 [13]. All of the above evidence supports an induced-fit, alternating access model of Na^+-dicarboxylate co-transport [6,14].

For the vcINDY dimer, this transport mechanism implies that the two clusters of helices at the protomer-protomer interface (TMs 2, 3, 7 and 8 from both protomers) form an anchoring scaffold for the transporter in the membrane (Fig. 1d and Supplementary Fig. 17). Connected by TM4a and TM9a as their respective hinges, the two helical bundles in the N- and C-terminal hands move up and down relative to the anchoring scaffold in opposite directions along the membrane normal (Supplementary Fig. 9), realizing an alternating access model of substrate translocation across the membrane.

As the bound citrate in our vcINDY structure is exposed to the cytosolic space, the structure represents the transporter's inward-facing, substrate-bound conformation, C_i-S-Na^+ [14]. This interpretation is also in agreement with our observations that citrate interacts with the transporter in solution but inhibits its transport activity only slightly from outside of the cell (Fig. 1b and Supplementary Fig. 5). It follows that citrate is a C_i-conformation specific inhibitor. As an importer, the low energy state of vcINDY in the absence of substrate should be the outward-facing conformation, C_o. Following Na^+ and substrate binding, the transporter converts from the

C_o-S-Na^+ state to the C_i-S-Na^+ state for cytosolic release. In the present work, however, because a high concentration of citrate was present in the crystallization buffer, a pre-release C_i state of the transporter was captured in the crystal structure.

The vcINDY structure reported here represents its inward-facing, C_i-S-Na^+ conformation, a pre-release state (Supplementary Fig. 17). As the protein functions as an importer, its substrate selectivity depends on the atomic structure of the substrate-binding site in its outward-facing C_o or C_o-Na^+ conformation, a pre-binding state. Between the outward- and inward-facing states, the binding sites for Na^+ ions are likely to be conserved. The interactions between the two SNT motifs and the two carboxyl groups at the ends of the substrate molecule are also likely to be conserved. Additional residues at the binding site that interact with the substitutions at the middle carbons probably provide the fine tuning of the substrate specificity of the transporter [9] that, for example, allows it to distinguish between different kinds of dicarboxylate molecules.

Substrate Specificity of sulfate transporters in the SLC13 family

The substrate-binding pocket in our crystal structure also explains the substrate preference between carboxylate transporters and sulfate transporters among SLC13 proteins [2-4]. In the sulfate transporters the substrate probably binds at the same location. At the third residue of the C-terminal SNT motif, in both NaS1 and NaS2, there is a proline residue there instead of a threonine or a valine as found in the carboxylate transporters (Fig. 4c, Supplementary Fig. 3). Interestingly, when we mutated Thr379 in vcINDY into a proline, the transport of succinate became sensitive to sulfate competition (Fig. 4d, Supplementary Fig. 15). In addition, there is a conserved serine residue at the vcINDY-P201 position among sulfate transporters. Previous

studies have shown that a substitution of the serine by alanine in the human NaS1 resulted in an increased K_m for sulfate transport [13].

Comparison with CNT

Although the amino acid sequence varies, the structure of the hairpin tip – capping loop motif is conserved between the two proteins, suggesting that this structural motif may be a common Na^+-binding motif in membrane transporter proteins. While vcINDY and CNT share a similar core structure, the ways by which each core is linked to its respective scaffold are completely different. CNT forms a trimer, with three pairs of long helices forming a scaffold around the threefold axis, which links to the core from each protomer (Supplementary Fig. 16). In contrast, in the dimeric vcINDY, the two palms in the core are each connected by a hinge to the anchoring thumbs, which cluster around the center of the dimer. The helical bundle of the palm forms a relatively well-defined structure for Na^+ binding, with the substrate sitting between the two oppositely-inverted palms. While the flexible linker between the palm and the thumb allows the two hands to change shape in a symmetrical manner [15], the anchoring scaffold formed by the thumbs at the center of the dimer allows the N- and C-terminal palms to move up and down in opposite directions in the membrane to propel substrate translocation. Such domain movement relative to an anchor scaffold during substrate translocation has been observed previously in the trimeric Na^+-dependent glutamate transporter [16].

References

1 Wright, E.M., Transport of carboxylic-acids by renal membrane-vesicles. *Ann Rev Physiol* **47**, 127-141 (1985).

2 Pajor, A.M., Sodium-coupled transporters for Krebs cycle intermediates. *Ann Rev Physiol* **61**, 663-682 (1999).

[3] Markovich, D. & Murer, H., The SLC13 gene family of sodium sulphate/carboxylate cotransporters. *Pflug Arch Eur J Phy* **447**, 594-602 (2004).
[4] Pajor, A.M., Molecular properties of the SLC13 family of dicarboxylate and sulfate transporters. *Pflug Arch Eur J Phy* **451**, 597-605 (2006).
[5] Wright, S.H., Hirayama, B., Kaunitz, J.D., Kippen, I., & Wright, E.M., Kinetics of sodium succinate cotransport across renal brush-border membranes. *J Biol Chem* **258**, 5456-5462 (1983).
[6] Yao, X. & Pajor, A.M., The transport properties of the human renal Na^+-dicarboxylate cotransporter under voltage-clamp conditions. *Am J Physiol Renal Physiol* **279**, F54-64 (2000).
[7] Hall, J.A. & Pajor, A.M., Functional characterization of a Na^+-coupled dicarboxylate carrier protein from *Staphylococcus aureus*. *J Bacteriol* **187**, 5189-5194 (2005).
[8] Hall, J.A. & Pajor, A.M., Functional reconstitution of SdcS, a Na^+-coupled dicarboxylate carrier protein from *Staphylococcus aureus*. *J Bacteriol* **189**, 880-885 (2007).
[9] Strickler, M.A., Hall, J.A., Gaiko, O., & Pajor, A.M., Functional characterization of a Na^+-coupled dicarboxylate transporter from *Bacillus licheniformis*. *Bba-Biomembranes* **1788**, 2489-2496 (2009).
[10] Pajor, A.M., Krajewski, S.J., Sun, N., & Gangula, R., Cysteine residues in the Na^+/dicarboxylate co-transporter, NaDC-1. *Biochem J* **344**, 205-209 (1999).
[11] Pajor, A.M., Conformationally sensitive residues in transmembrane domain 9 of the Na^+/dicarboxylate co-transporter. *J Biol Chem* **276**, 29961-29968 (2001).
[12] Pajor, A.M. & Randolph, K.M., Conformationally sensitive residues in extracellular loop 5 of the Na^+/dicarboxylate co-transporter. *J Biol Chem* **280**, 18728-18735 (2005).
[13] Li, H. & Pajor, A.M., Serines 260 and 288 are involved in sulfate transport by hNaSi-1. *J Biol Chem* **278**, 37204-37212 (2003).
[14] Law, C.J., Maloney, P.C., & Wang, D.N., Ins and outs of major facilitator superfamily antiporters. *Annu Rev Microbiol* **62**, 289-305 (2008).
[15] Forrest, L.R. & Rudnick, G., The rocking bundle: a mechanism for ion-coupled solute flux by symmetrical transporters. *Physiology (Bethesda, Md* **24**, 377-386 (2009).
[16] Reyes, N., Ginter, C., & Boudker, O., Transport mechanism of a bacterial homologue of glutamate transporters. *Nature* **462**, 880-885 (2009).

Supplementary Table 1. Crystallographic data collection and reduction statistics for phasing

Data set	1	2	3	4	All (1-4)
Unit-cell parameters a, b, c (Å) β (°)	101.42, 101.41, 165.12 101.96	101.56, 101.64, 165.73 102.12	101.73, 101.04, 165.50 101.58	102.83, 100.85, 165.74 100.78	101.88, 101.24, 165.53 101.61
Number of frames	360	360	360	360	1,440
Bragg spacings (Å)	40-3.5 (3.59-3.5)	40-3.7 (3.8-3.7)	40-4.0 (4.1-4.0)	40-4.0 (4.1-4.0)	40-3.5 (3.59-3.5)
Measurements	313,099	258,201	213,160	199,285	1,002,530
Unique reflections	41,571	34,565	28,103	28,068	41,621
Multiplicity	7.5 (7.3)	7.5 (6.2)	7.6 (7.4)	7.1 (7.4)	24.1 (7.4)
Completeness (%)	99.3 (93.2)	98.2 (74.9)	99.8 (100.0)	99.6 (100.0)	99.4 (94.1)
R_{merge}[1]	0.090 (0.609)	0.146 (0.906)	0.145 (0.650)	0.181 (0.727)	0.246 (0.632)
I/σ(I)[2]	19.1 (3.8)	12.6 (2.6)	17.6 (4.5)	11.9 (3.8)	19.3 (3.8)
ΔF/σ(ΔF)[3]	1.97 (0.91)	1.32 (0.72)	1.43 (0.68)	1.18 (0.74)	1.91 (0.92)
Anomalous CC[4] (%)	85.6 (17.6)	73.2 (4.4)	63.5 (4.8)	60.1 (0.4)	83.0 (14.2)

Notes:
[1]$R_{merge} = \Sigma_{hkl} \Sigma_i |I_i^{hkl} - \langle I^{hkl} \rangle| / \Sigma_{hkl} \Sigma_i I_i^{hkl}$, where I is the intensity of a reflection hkl and <I> is the average over measurements of hkl.
[2]$I/\sigma(I) = \langle\langle I^{hkl} \rangle / \sigma(\langle I^{hkl} \rangle)\rangle$ where $\langle I^{hkl} \rangle$ is the weighted mean of all measurements for a reflection hkl and $\sigma(\langle I^{hkl} \rangle)$ is the standard deviation of the weighted mean. The values are as reported from *SCALA* as Mn(I/sd).
[3]ΔF/σ(ΔF) is average anomalous signal from data truncated to d_{min} = 4 Å. The values are derived by using CCP4 programs and are computed as $\langle |\Delta F| / \sigma(\Delta F) \rangle$ where ΔF = |F(h)| - |F(-h)|.
[4]Anomalous correlation coefficient evaluated from data truncated to d_{min} = 4 Å.
Values in parentheses are from the highest resolution shell.

Supplementary Table 2. Crystallographic data collection and refinement statistics

	Crystal #1
Data collection	
Space group	$P2_1$
Unit-cell dimensions	
a, *b*, *c* (Å)	101.42, 101.41, 165,12
α, β, γ (°)	90, 101.96, 90
Resolution (Å)	50.00-3.21 (3.27-3.21)*
R_{merge}	9.8 (92.3)
$I / \sigma(I)$	11.71 (1.51)
Completeness (%)	97.9 (83.3)
Redundancy	3.9 (3.5)
Refinement	
No. reflections	52,199
R_{work} / R_{free}	0.2280/0.2913
No. atoms	12390
Protein	12263
Ligand	39
Sodium	4
B-factors	98.66
Protein	98.42
Ligand	127.02
Sodium	66.43
R.m.s. deviations	
Bond lengths (Å)	0.010
Angles (°)	1.557
Ramachandran statistics (%)	
Favored	88.1
Outliers	0.2

Notes: *: A single crystal was used for the structure.
$R_{merge} = \Sigma_{hkl} \Sigma_i |I_i^{hkl} - \langle I^{hkl} \rangle| / \Sigma_{hkl} \Sigma_i I_i^{hkl}$, where I is the intensity of a reflection hkl and <I> is the average over measurements of hkl.
Redundancy represents the ratio between the number of measurements and the number of unique reflections.
R factor = $\Sigma|F(\text{obs}) - F(\text{cal})|/\Sigma F(\text{obs})$; 5% of the data that were excluded from the refinement were used to calculate R_{free}. The average *B* factor was calculated for all non-hydrogen atoms.
r.m.s.d. of bond is the root-mean-square deviation of the bond angle and length.
Numbers in parentheses are statistics of the highest resolution shell.

Supplementary Table 3. Distances between Na^+ ion and protein coordinating atoms

Coordinating atoms*	**Distance to Na^+ (Å)**
S146 carbonyl O	2.34
S146 hydroxyl O	2.53
S150 carbonyl O	3.33
N151 amide O	2.36
G199 carbonyl O	3.26

Notes: *: Interatomic distances were measured using Chain D.

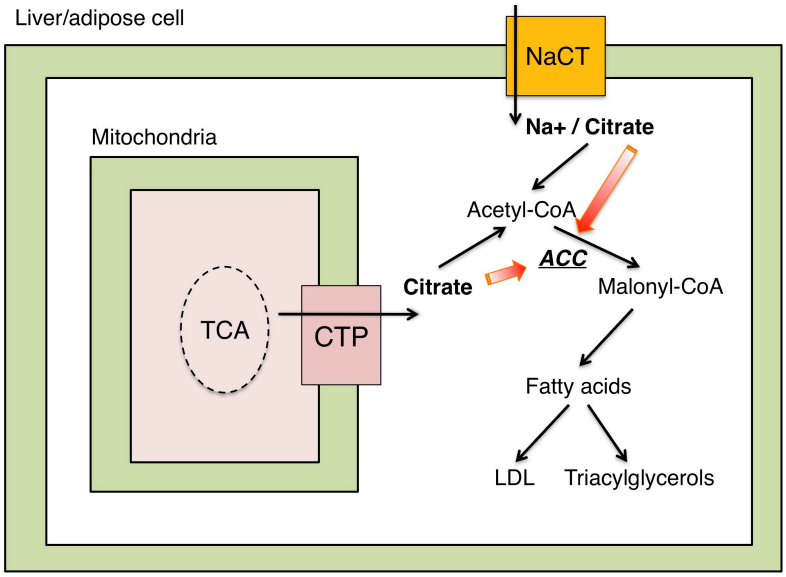

Supplementary Fig. 1. Pathway for fatty acid biosynthesis in liver and fat cells. The rate of fatty acid synthesis depends on the cytosolic citrate level. NaCT, Na^+-dependent plasma membrane citrate transporter; TCA, citric acid cycle; CTP, mitochondrial citrate transporter;
ACC, acetyl CoA carboxylase; LDL, low-density lipoprotein.

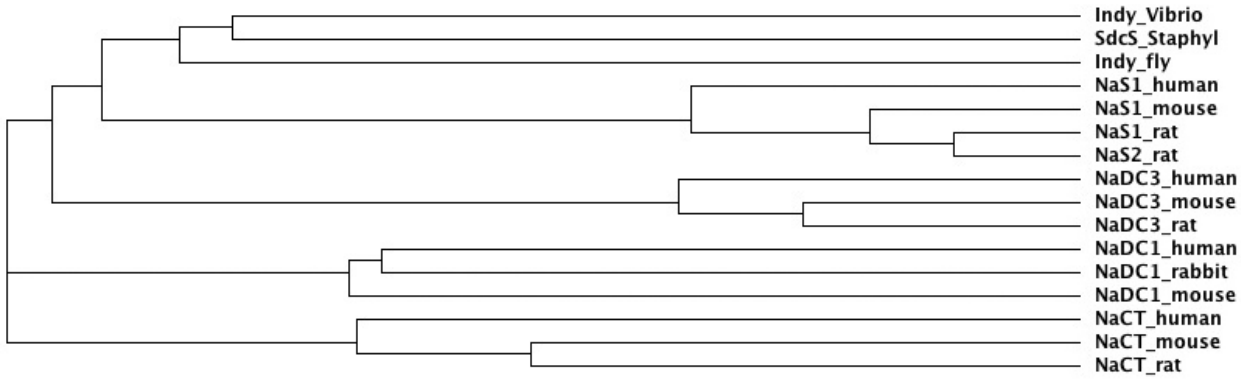

Supplementary Fig. 2. Phylogenetic tree of the DASS family.

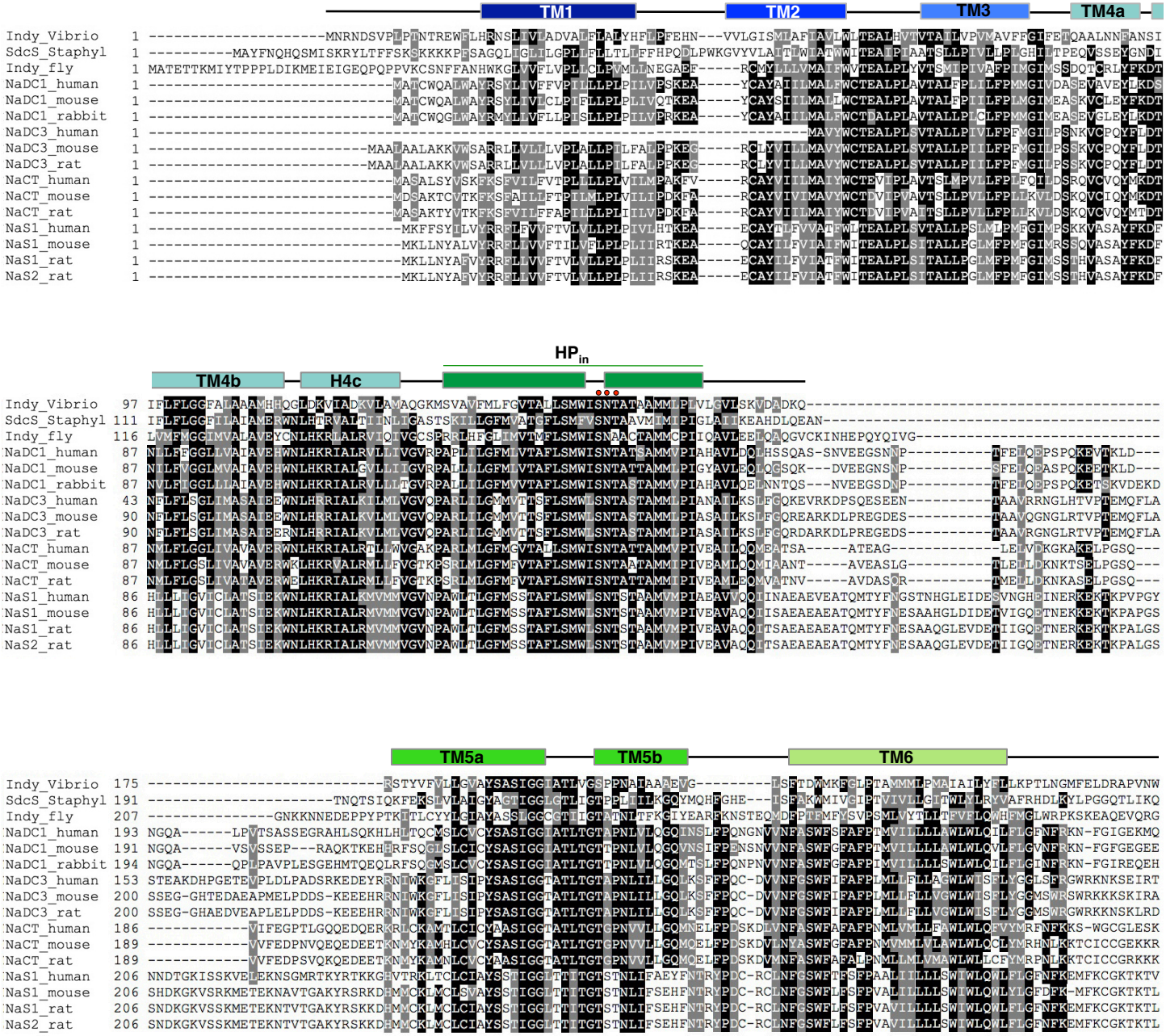

(Supplementary Fig. 3. Continued)

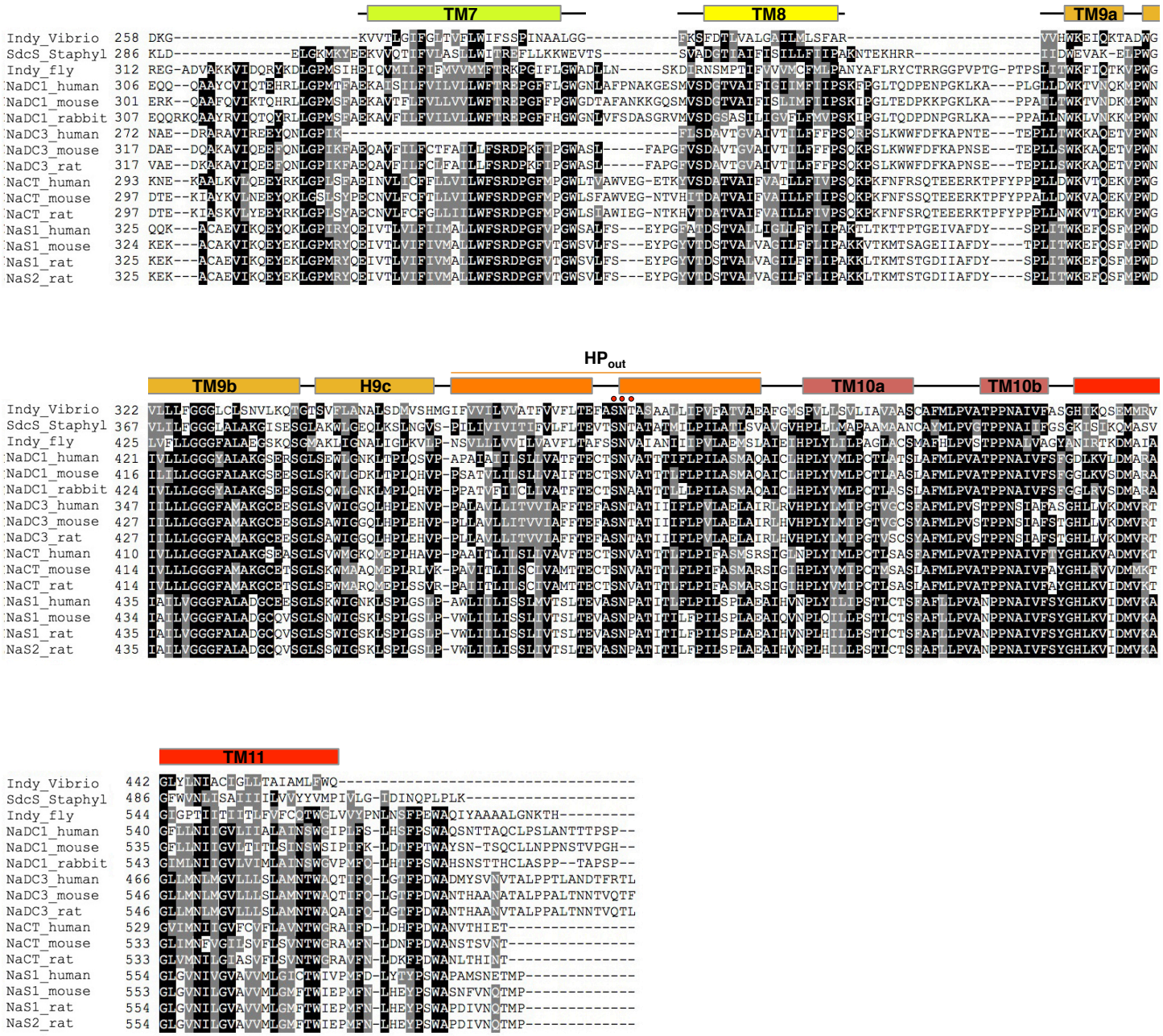

Supplementary Fig. 3. Amino acid sequence alignment of vcINDY and its homologs. Positions of secondary structures of the protein as observed in its crystal structure are indicated, and they are colored using the same rainbow schemes as in Figs. 1-4. The red dots indicate the two SNT motifs for carboxyl group binding.

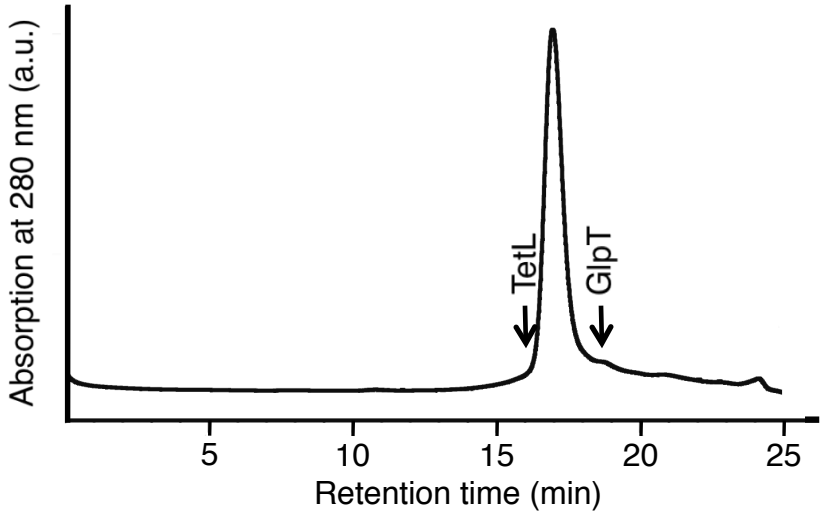

Supplementary Fig. 4. Analytical size-exclusion chromatography trace of purified vcINDY in dodecylmatoside detergent. vcINDY ran as a single, monodisperse peak at 16.951 mins. The retention times of the monomeric glycerol-3-phosphate transporter (GlpT, 18.654 mins) and the dimeric tetracycline transporter (TetL, 16.133 mins), two membrane transporter proteins with a similar molecular weight as vcINDY, are indicated.

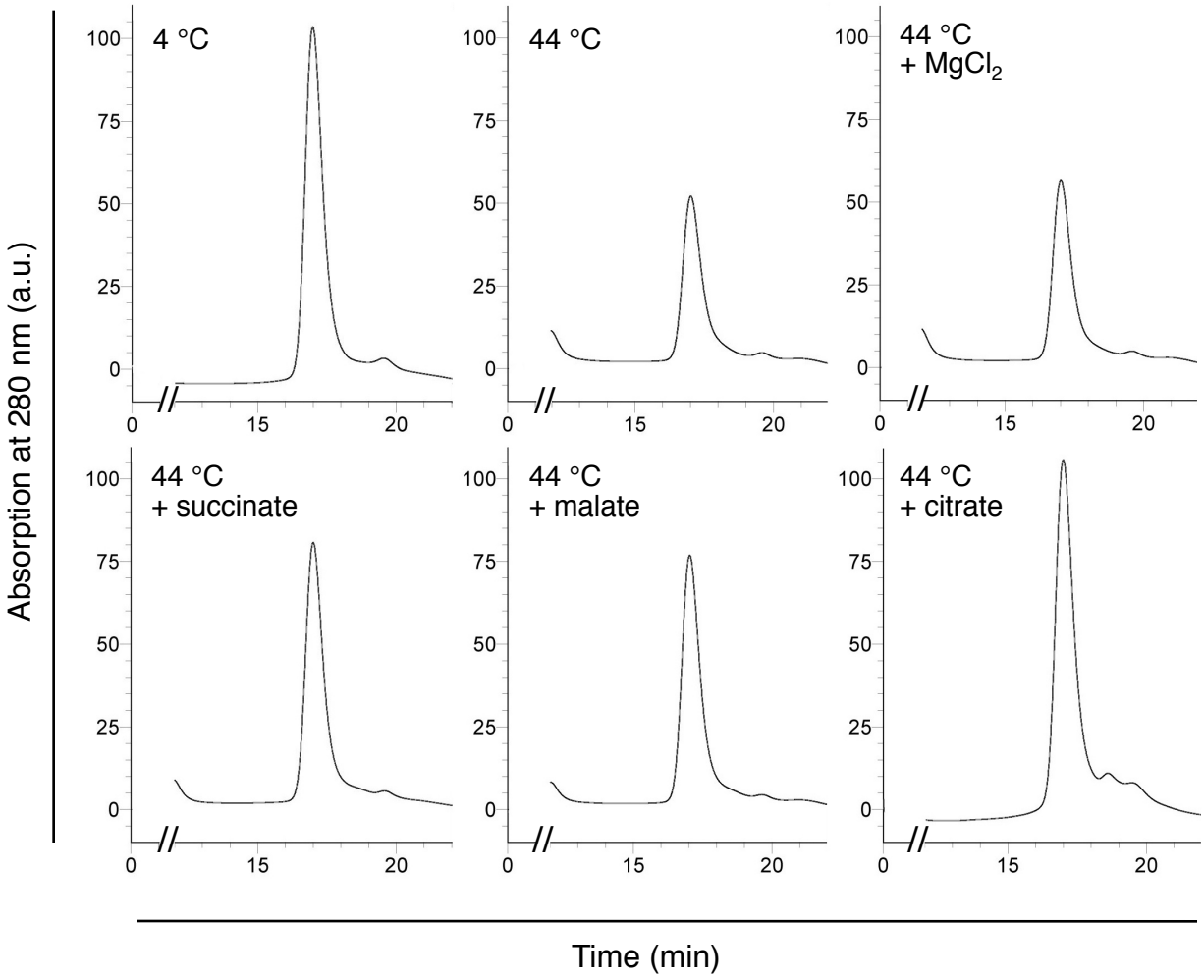

Supplementary Fig. 5. Effects of various salts on the thermostability of purified vcINDY characterized by analytical size-exclusion chromatography. vcINDY purified in DDM detergent and 100 mM NaCl ran as a sharp peak (without NaCl, the protein would aggregate). Upon being heated to 44 °C for 10 minutes, the peak height dropped by ~50%. The presence of succinate or malate during incubation was able to stabilize the protein. The largest effect in thermostabilization was observed for citrate, in which the peak height was completely recovered, indicating a specific interaction between the transporter and citrate. As a control, $MgCl_2$ had no effect. The void was at ~11 mins.

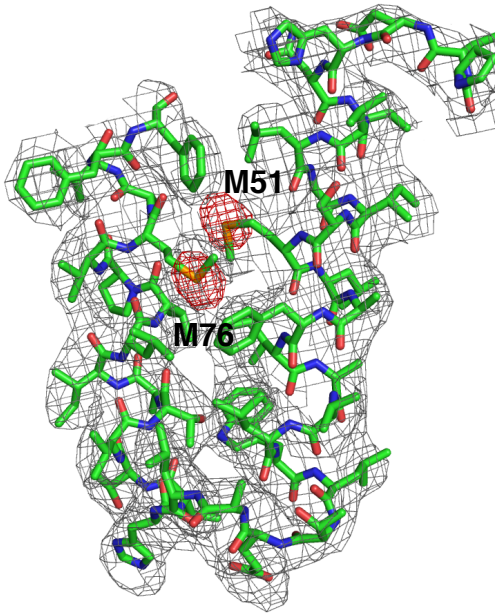

Supplementary Fig. 6. Quality of vcINDY electron density maps. The $2F_o - F_c$ map (contoured at 1.5σ) is superimposed with the anomalous difference Fourier map (contoured at 3.7σ) of the SeMet crystal, which was used to identify the position of 22 out of the 23 methionine residues of the vcINDY protein. The crystallographic asymmetric unit cell contains four vcINDY protomers.

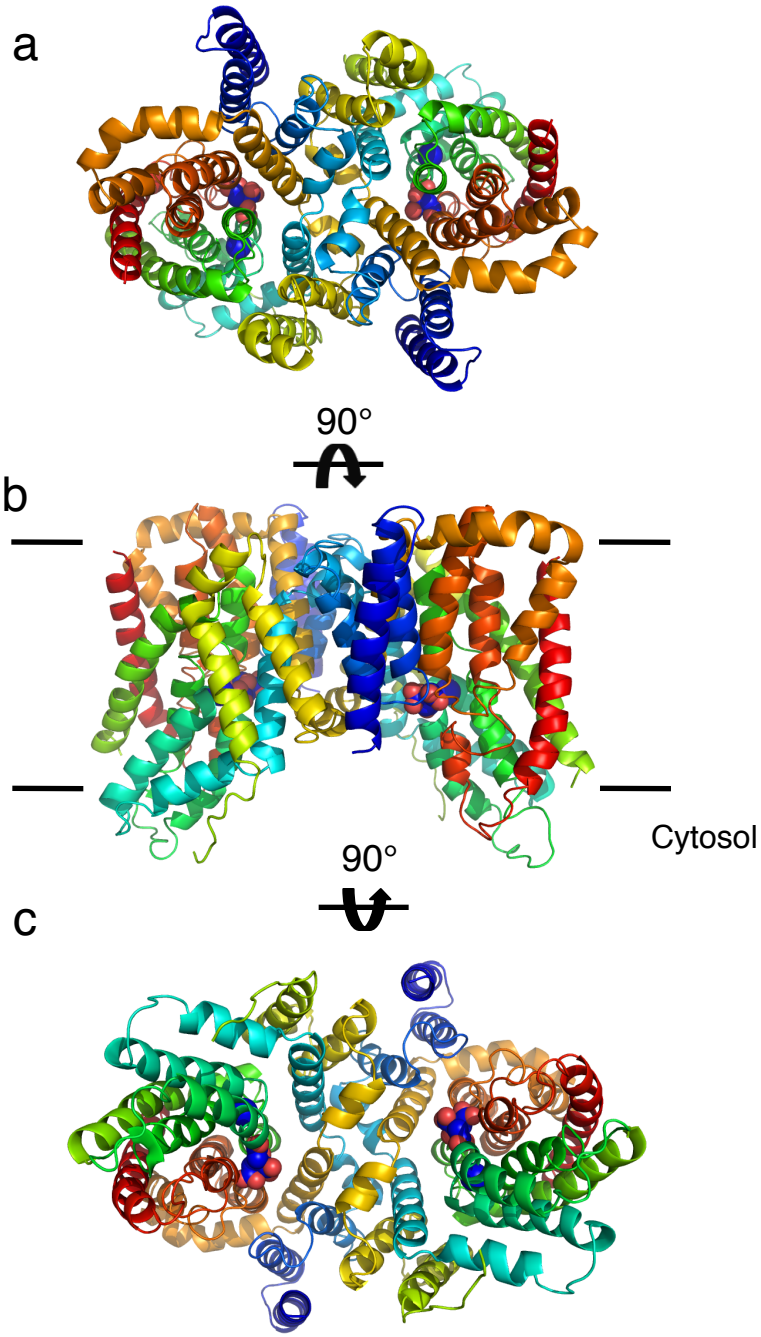

Supplementary Fig. 7. Periplasmic view of the vcINDY dimer. Structure of the protein is viewed from the extracellular space. The cross section of the protein dimer in the membrane plane measures about 80 Å by 55 Å, whereas the height of the protein along the membrane normal is 60 Å. Many residues at the interface are conserved from bacteria to mammals, including Trp320, which forms an inter-protomer π-π interaction with the Trp320 of the other protomer.

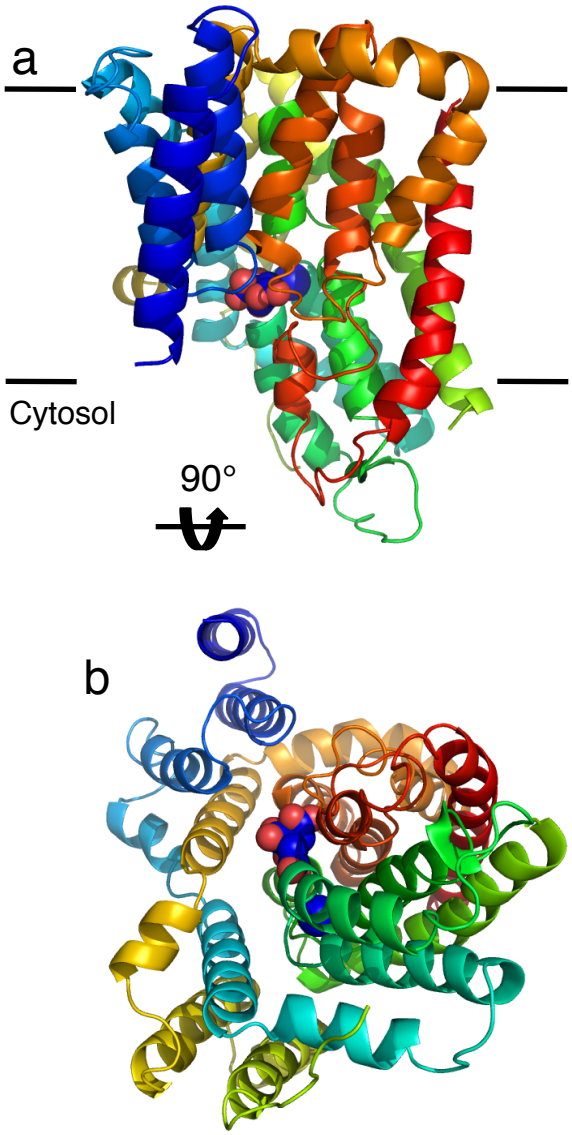

Supplementary Fig. 8. Structure of the vcINDY protomer. **a**, Viewed from within the membrane. **b**, Viewed from the cytosol.

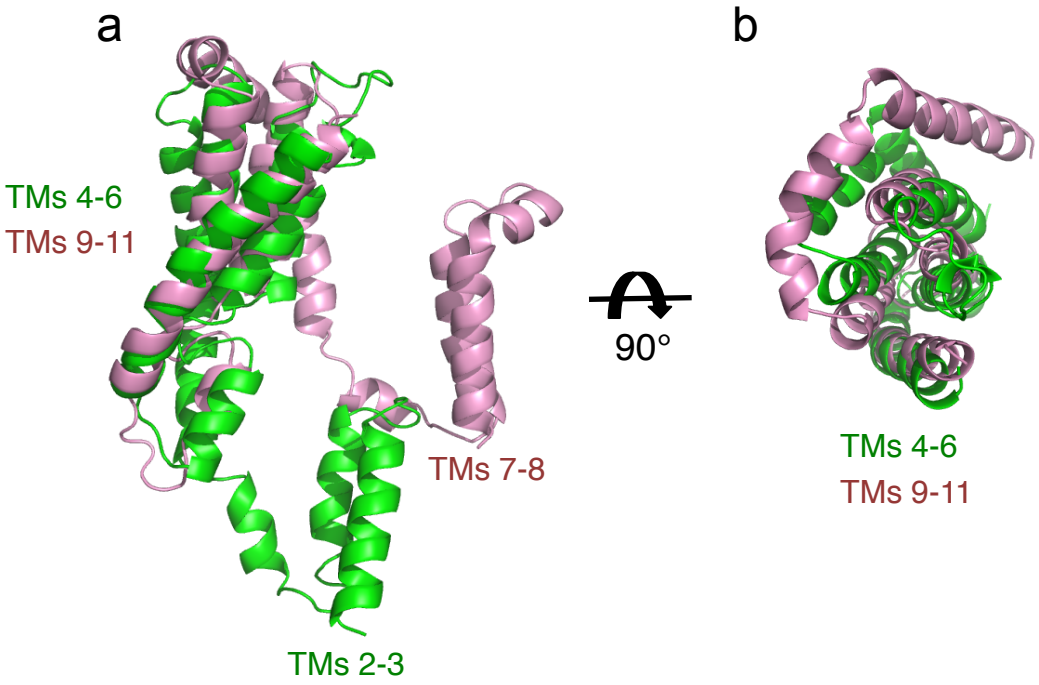

Supplementary Fig. 9. Comparison of the N-terminal and C-terminal halves in vcINDY. **a**. Overlay of the N- and C-terminal halves, with their helical bundles superimposed. **b**. Overlay of the N- and C-terminal helical bundles.

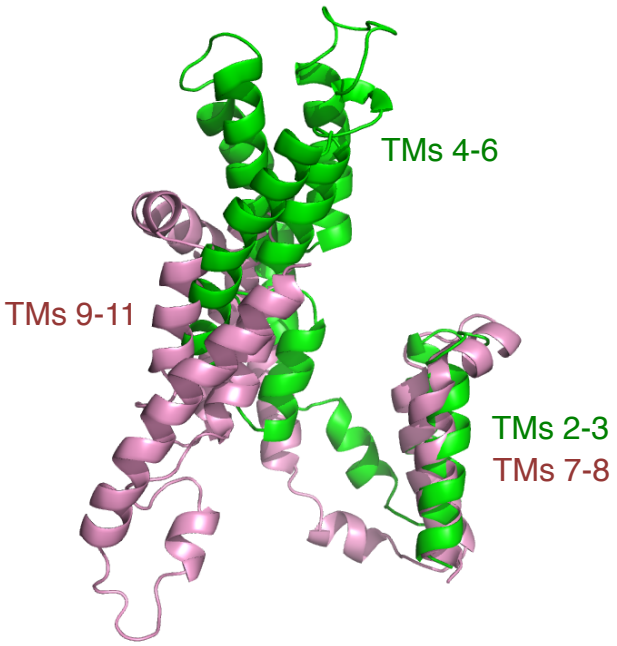

Supplementary Fig. 10. Comparison of the N-terminal and C-terminal halves of the vcINDY structure. Overlay of the N- and C-terminal halves, with their thumbs superimposed.

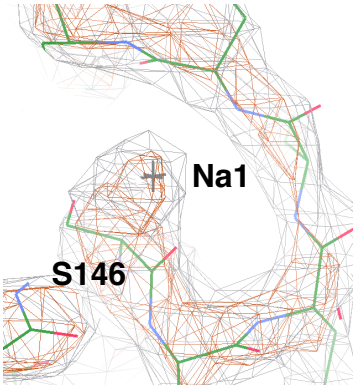

Supplementary Fig. 11. Electron density ($2F_o - F_c$ map, contoured at 2.5σ and 3.5σ) for the bound Na^+ ion at the Na1 site. The electron density between the hairpin HP_{in} tip and the loop L5ab is too large for a Li^+ ion, and its ligand coordination and the conservation of the coordinating amino acid sequence do not support a bound water molecule. Therefore, we infer that the density belongs to a bound Na^+ ion.

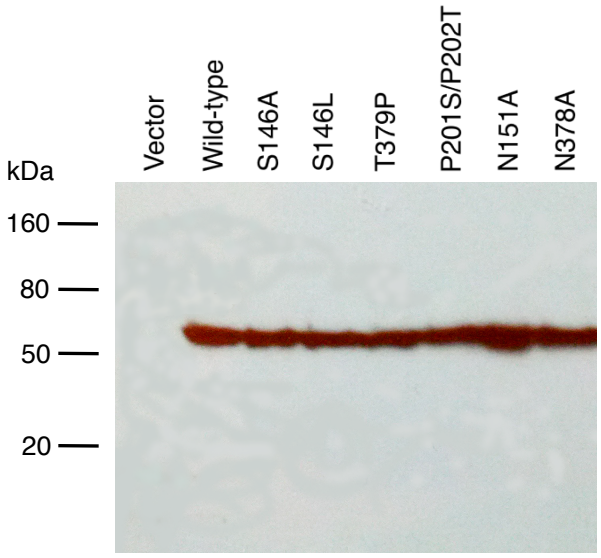

Supplementary Fig. 12. Western blot analysis of expression levels of vcINDY mutants in *E. coli* for uptake experiments. Most of the mutants expressed at comparable levels to the wild-type protein, indicating that any decrease observed in transport activity was not due to reduced protein expression.

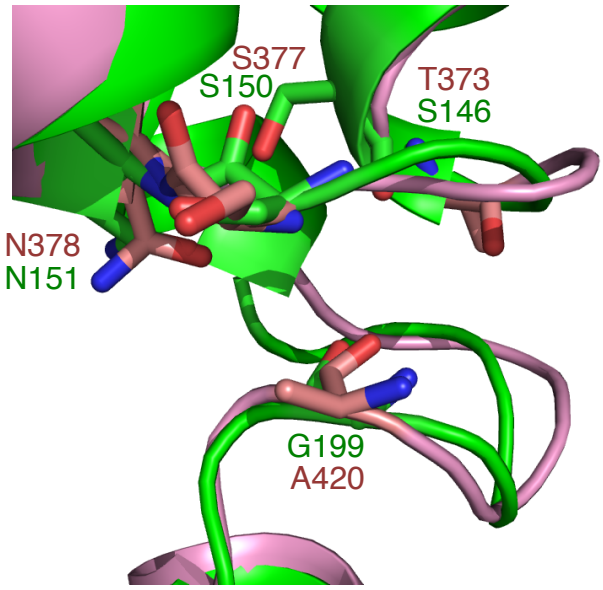

Na1 site (green)	Na2 site (pink)
S146 (Cα) - N151 (s.c.) 4.6 Å	T373 (Cα) to N378 (s.c.) 6.7 Å
S146 (s.c.) - N151 (s.c.) 3.1 Å	T373 (s.c.) to N378 (s.c.) 7.6 Å
G199(Cα) - S150 (Cα) 6.6 Å	A420 (Cα) to S377 (Cα) 8.1 Å

Supplementary Fig. 13. Overlay of Na1 and Na2 site structures and comparison of distances between the corresponding hairpin tip and capping loop. The distances between the HP_{out} and L10ab in the C-terminal Na2 clamshell (pink) is significantly larger than the corresponding distances between the HP_{in} and L5ab in the N-terminal Na1 clamshell (green), supporting the hypothesis that a Na^+ ion has been released from the Na2 site. s.c. denotes side chain.

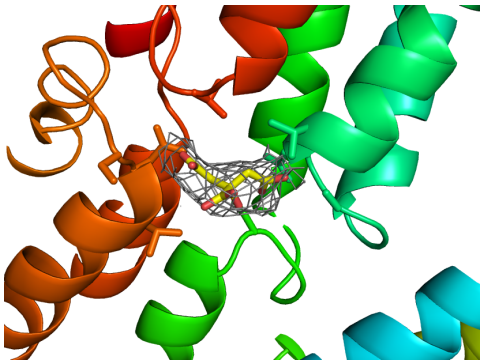

Supplementary Fig. 14. Electron density ($2F_o - F_c$ map, contoured at 1.0σ) for the bound citrate molecule.

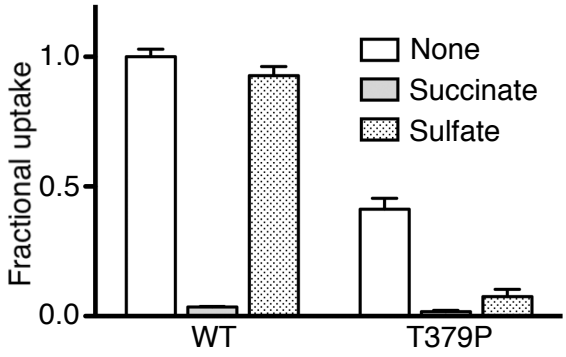

Supplementary Fig. 15. Succinate transport activity of wild-type and mutant vcINDY in the presence of sulfate. $N = 3$.

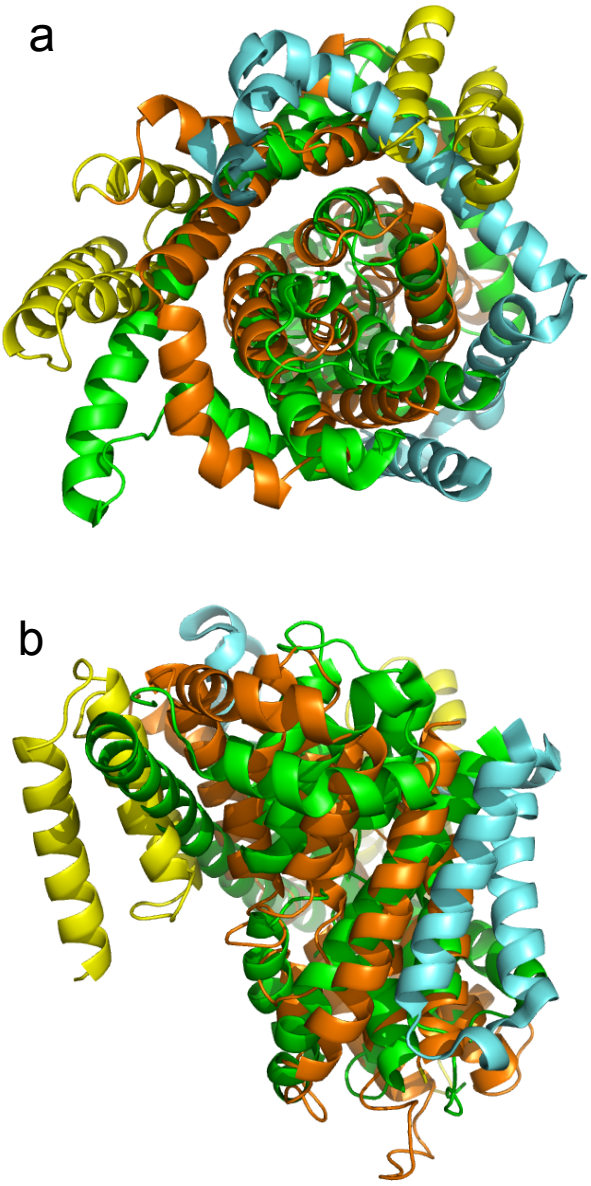

Supplementary Fig. 16. Comparison of the vcINDY protomer structure with that of the concentrative nucleotide transporter (CNT) from *Vibrio cholerae*. vcINDY is colored orange and yellow, whereas CNT is colored green and cyan. **a**, Periplasmic view. **b**, Viewed from within the membrane. The r.m.s.d between Cα atoms of these most conserved parts, the helical hairpins and the two Transmembrane helices that follow them, is 4.9 Å for those 243 amino acid residues.

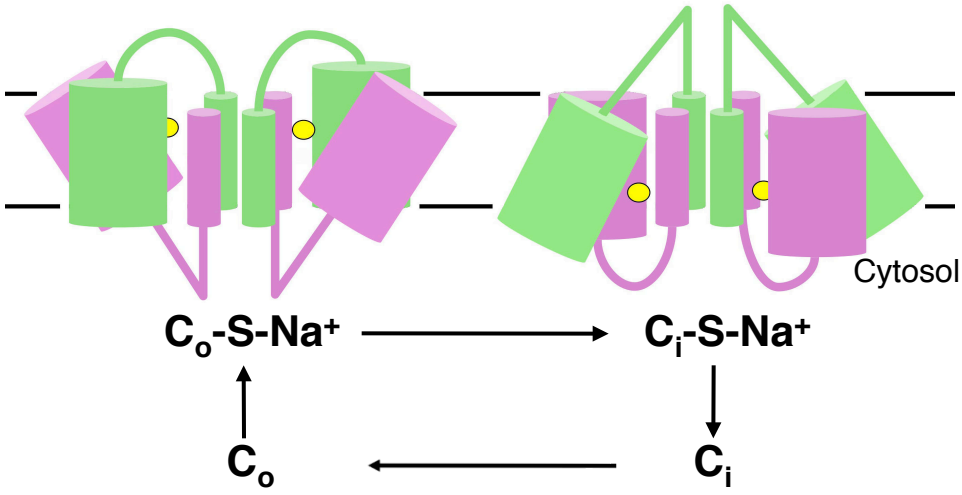

Supplementary Fig. 17. Proposed transport mechanism of vcINDY. In the outward-facing C_o conformation, the N-terminal half adopts a U-shape, whereas the C-terminal half adopts a V-shape. Following Na^+ and substrate binding, the N- and C-terminal halves change to a V- and a U-shape, respectively, resulting in the inward-facing C_i-S-Na^+ conformation. After the release of Na^+ and substrate to the cytosol, the transporter returns to the C_o state, completing a substrate translocation cycle.